Intruders in the Dust: Air-Driven Granular Size Separation

Matthias E. Möbius,[1] Xiang Cheng,[1] Greg S. Karczmar,[2] Sidney R. Nagel,[1] and Heinrich M. Jaeger[1]
[1]*The James Franck Institute and Department of Physics, The University of Chicago, Chicago, Illinois 60637, USA*
[2]*Department of Radiology, The University of Chicago, Chicago, Illinois 60637, USA*
(Received 13 May 2004; published 1 November 2004)

Using MRI and high-speed video we investigate the motion of a large intruder particle inside a vertically shaken bed of smaller particles. We find a pronounced, nonmonotonic density dependence, with both light and heavy intruders moving faster than those whose density is approximately that of the granular bed. For light intruders, we furthermore observe either rising or sinking behavior, depending on intruder starting height, boundary condition, and interstitial gas pressure. We map out the phase boundary delineating the rising and sinking regimes. A simple model can account for much of the observed behavior and shows how the two regimes are connected by considering pressure gradients across the granular bed during a shaking cycle.

DOI: 10.1103/PhysRevLett.93.198001 PACS numbers: 45.70.Mg, 64.75.+g, 83.80.Fg

Unlike thermal systems, which favor mixing to increase entropy, granular systems tend to separate under an external driving mechanism such as vibrations [1,2]. This is commonly known as the Brazil Nut Effect, in which a large particle, the "intruder," rises to the top of a bed of smaller background particles [3–5]. More recently, new behavior was discovered for the limit of very small bed particles ("dust"), in particular, the sinking of light intruders [6,7], and a nonmonotonic dependence of the rise time on density [8–10]. A number of theory and experimental papers explored different aspects of this surprising behavior [11–16], but so far there has been no consensus about either the underlying mechanisms or the relative importance of various system parameters in driving the intruder motion.

Here we present results from a systematic investigation of both the intruder motion and the bed particle flow. Our central finding is a phase diagram that delineates rising and sinking behaviors of the intruder as a function of interstitial gas pressure, intruder density, and initial intruder height within the container. Our results lead to a physical model that provides a unifying framework to describe both rising and sinking regimes. This connects previously disjointed pieces of a puzzle that pointed to the importance of pressure gradients [7–9] but approached the two regimes as separate phenomena. As a consequence, our findings directly contrast with the mechanisms proposed in Refs. [6,10,14,16] that neglect interstitial gas flow.

We placed granular material of total height H, with an individual grain density ρ_m and packing fraction ϕ, inside an acrylic cylinder (inner diameter 8.2 cm) mounted on a shaker and used individual, well-spaced "taps" to vibrate the vessel vertically. Each tap is a single, full period of a sine wave with frequency f and amplitude A. The cell could be evacuated to a gas pressure P. Both smooth and rough cells (created by gluing glass beads to the interior walls of an otherwise smooth cell) were used to study the effect of wall friction. A large intruder sphere of diameter D was buried in the bed of background spheres (diameter d) at a height h_s measured from the vessel bottom to the intruder top. A range of diameter ratios D/d, shaking parameters, and background particle materials [glass, zirconium oxide, tapioca, and seeds (for magnetic resonance imaging)] were investigated. The intruder density, ρ, could be tuned by filling a hollow sphere with different materials. We measured the number of taps required for the intruder to break through the upper free surface, T_{rise}, or to reach the bottom, T_{sink}. In addition, the intruder position could be recorded with high-speed video throughout the shaking process by attaching to the intruder a thin, vertical straw extending above the upper surface. We verified that the straw did not affect the intruder motion.

To track the evolution of both the intruder and the surrounding bed material we used magnetic resonance imaging (MRI). Figure 1 shows how the intruder motion is coupled to the background convection in a rough cell.

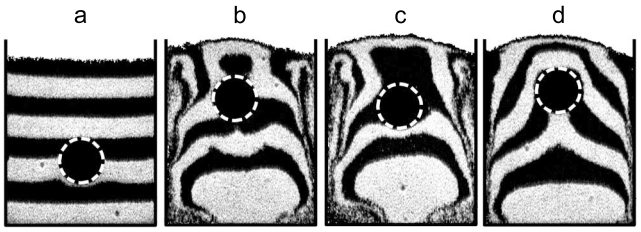

FIG. 1. MRI images of a large intruder sphere ($D = 25$ mm) rising in a bed of smaller particles. Images are vertical cuts through the center of the container. (a) Layered bed and starting position of the intruder before shaking. (b)–(d) Size separation in the presence of convection for intruders of three different densities at $\Gamma = 5$, $f = 13$ Hz: (b) $\rho/\rho_m = 0.08$ after 23 taps; (c) $\rho/\rho_m = 0.44$ after 30 taps; and (d) $\rho/\rho_m = 2.33$ after 11 taps. Here $\rho_m = 1.10$ g/ml is the average density of individual seeds. The average seed diameter is 0.8 mm.

Horizontal layers of poppy seeds (MRI active) were alternated with layers of rajagara seeds (MRI inactive), with the intruder initially placed on the lowest black layer [Fig. 1(a)]. Figures 1(b)–1(d) show the situation, for intruders with progressively higher densities, after several taps when the intruder had risen slightly more than its own diameter. In both Figs. 1(b) and 1(d), the intruders move faster relative to the dark layer on which they were originally placed. In Fig. 1(c), the intermediate weight intruder with density close to the effective density, $(\phi\rho_m)$, of the bed remains at the same relative position to that layer. Thus, its rise time corresponds to the convection speed of the bed particles immediately below it. Above the intruder in Figs. 1(b) and 1(c), the alternating light and dark layers are no longer horizontal, because convection speeds up near the free surface [5] and convection rolls churn the material into a swirl pattern near the side walls. In Fig. 1(d), the dense intruder rises so rapidly that these convection rolls have not had a chance to move the background material appreciably. As the dense intruder rises, it pushes a wedge-shaped volume of material above it and creates a wake below it. In Fig. 1(b) for the light intruder, there is no sign of a similar wake.

One aspect common to prior observations of the sinking regime is the need for small bed particle sizes, typically $d \leq 0.5$ mm [6,7]. However, this is precisely also the size regime in which it becomes very difficult to excite axisymmetric bed flow patterns [17]. In general, wall-driven convection sets up axisymmetric convection rolls in the bed [5,17]. However, when either bed permeability or wall-driven friction is sufficiently reduced, the convection becomes asymmetric [17,18] so that intruders are driven towards the cell wall. We find the onset of asymmetric flow for $d \leq 0.35$ mm in the rough cell and $d \leq 0.5$ mm in the smooth cell. In the following, we focus on representative results obtained with $d = 0.5$ mm glass beads ($\rho_m = 2.5$ g/ml), $D = 25$ mm intruders, bed fill height $H = 85$ mm, and dimensionless shaking acceleration $\Gamma = A(2\pi f)^2/g = 5$ at $f = 13$ Hz. The two cell types then allow us to investigate how the overall bed flow affects the intruder motion.

Despite the clearly different flow patterns in the two cells, we find a qualitatively similar dependence of the intruder rise time, T_{rise}, on the ratio of intruder density, ρ, to ρ_m (Fig. 2). In general, the effect increases with increasing D [8,18]. For both boundary conditions, at ambient pressure, T_{rise} has a pronounced peak at $\rho^* \sim 0.5\rho_m$, which is close to the effective density $(\phi\rho_m)$. On either side of this peak, there is a large increase of the intruder velocity (i.e., a decrease in T_{rise}). When P is decreased, the peak amplitude shrinks and ρ^* moves to smaller values as shown for both cells in the inset of Fig. 2(a). From MRI measurements (Fig. 1), we know that at the peak ρ^* the intruder rises with the convection, while intruders on either side of the peak rise faster. This differs from previous experiments [8,10] which measured con-

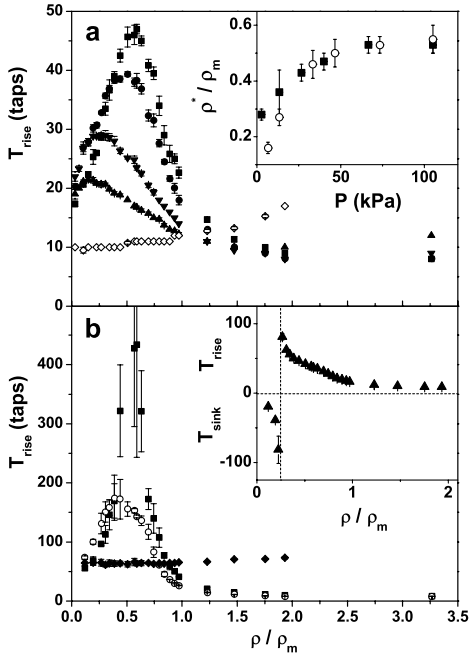

FIG. 2. (a) Intruder rise time T_{rise} versus relative density ρ/ρ_m at different pressures P. (a) Rough cell: ■, 101 kPa; ●, 47 kPa; ▼, 13 kPa; ▲, 6.7 kPa; ◇, 0.13 kPa. Inset: rise-time peak or divergence position, ρ^*/ρ_m, as a function of P in the rough ○ and smooth ■ cell. (b) Smooth cell: ■, 101 kPa; ○, 27 kPa; ◆, 0.13 kPa. Inset: Sinking regime at 2.7 kPa. In both cells, $h_s = 5.5$ cm.

vection without the intruder and did not account for the influence of the intruder on the bed. When P is lowered, convection speeds up so that the rise time at ρ^* shrinks (Fig. 2). For the rough cell, ρ^* decreases more strongly than in the smooth cell and at low P it is indistinguishable from $\rho^* = 0$, having reached our lowest measurable density. At sufficiently low pressure ($P \leq 0.13$ kPa), the nonmonotonic behavior in T_{rise} disappears and the curve is featureless. The slow increase in T_{rise} as ρ increases we believe is due to the heavy intruder burrowing back into the bed at the end of each cycle. Aside from this, there is essentially no density dependence to the rise time. For $\rho < \rho^*$ and $P \sim 2.7$ kPa a dramatic change in behavior can be observed, seen most clearly in the smooth cell. As shown in the inset of Fig. 2(b), at $P = 2.7$ kPa, instead of speeding up again as ρ is lowered below ρ^*, the intruder stops rising and begins to sink. In this case, the peak in T_{rise} at ρ^* turns into a discontinuity as shown in the inset of Fig. 2(b). We find similar behavior in the rough cell but over a much smaller region of parameter space.

The transition between the two regimes of intruder rising and sinking is controlled by at least six main parameters: ρ/ρ_m, P, d, h_s, H, and cell wall roughness. This allows us to construct phase diagrams for different wall roughness as shown in Fig. 3, where we plot the maximum starting height for sinking, h_c, as a function of relative density. Results for different d and the relation

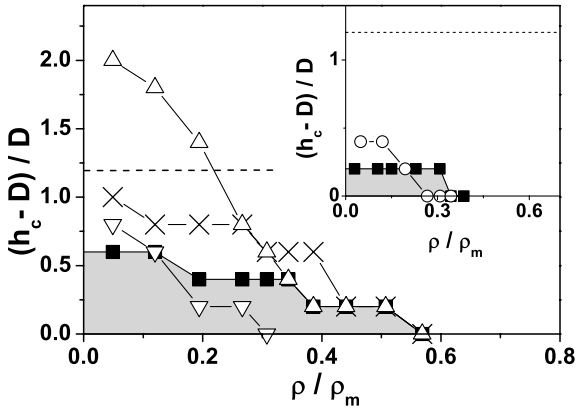

FIG. 3. Phase diagrams delineating the rising and sinking regimes for $d = 0.5$ mm beds at various pressures P. Above each phase boundary, intruders rise. Shaded areas show the sinking regime at ambient pressure. Main panel: ■, 101 kPa; ×, 27 kPa; △, 2.7 kPa; ▽, 0.67 kPa in the smooth cell. Inset: ■, 101 kPa; ○, 27 kPa in the rough cell. In both cells, all intruders rise from the bottom ($h_s = D$) when $P < 0.13$ kPa. The dashed lines indicate h_s of Fig. 2.

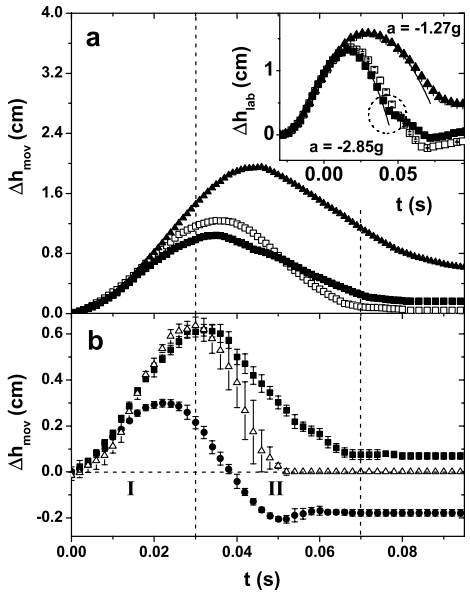

FIG. 4. Intruder displacement in the moving frame. Vertical dashed lines delineate part I and part II of the period (see text). (a) Three different densities with $h_s = 7.0$ cm in the rough cell. ■, $\rho/\rho_m = 0.043$; □, $\rho/\rho_m = 0.52 \simeq \rho^*/\rho_m$; ▲, $\rho/\rho_m = 3.3$. Inset: Same trajectories in the lab frame. The "kink" for the lightest intruder is highlighted by the dashed circle. (b) Light intruder ($\rho/\rho_m = 0.043$) in smooth cell rising at $h_s = 6.5$ cm $> h_c$ (■) and sinking at $h_s = 3.5$ cm $< h_c$ (●). The third curve (△) tracks the gap underneath the bed.

between H and h_c will be presented elsewhere [18]. If the intruder is placed close enough to the top surface, it will invariably rise. The regions where the intruder sinks depend on pressure, P, and, when they occur, happen at low relative densities, ρ/ρ_m, and low heights, h_s. Interestingly, the sinking regime is largest for intermediate pressures around 1–30 kPa. At lower pressure, it disappears and all particles rise at all depths as they are swept along via the background convection rolls. We find the sinking regime only for $\rho < \rho^*$.

In order to determine how the intruder interacts with the background, we measured its motion during flight using high-speed video. In Fig. 4, we plot the vertical displacement Δh (measured in the moving frame of the cell) versus time. The inset of Fig. 4(a) shows intruder trajectories in the lab frame. In both rough and smooth cells, the bed lifts off the cell bottom at $t = 0$, the particles near the walls land at 0.05 s and the condensation front of the bed reaches the intruder at ~0.07 s. Between liftoff and landing of the bed, the heavy intruder in the rough cell follows a parabolic trajectory with a total downward acceleration only slightly greater than g (Fig. 4, inset), whereas, as is evident from the larger effective downward acceleration, the lighter intruder experiences larger drag due to the air flow. Before landing, the light particles show a sharp change in behavior. This is seen as a kink in the curves occurring near 0.045 s (apparent in the lab frame). This kink, which slows down the landing of the light particles, appears to be responsible for the increase in upward velocity for $\rho < \rho^*$. In the smooth cell, the kink is not as dramatic as in the rough cell but the departure from the downward parabolic profile is still evident and the intruder clearly moves down slower than the bed. When a light intruder is in the sinking region of the phase diagram, its trajectory, as seen in Fig. 4(b), is pulled down with respect to the bed in the first part of the shaking period.

These results clearly identify the interstitial gas as the cause of the nonmonotonic behavior in T_{rise} and of the reversal from rising to sinking. They contradict several recent models that ignore air effects or treat the rising and sinking regimes as unrelated phenomena [10,14,16]. However, we can explain the rise-sink crossover in the phase diagram and predict quantitatively the peak at $T_{\text{rise}}(\rho^*/\rho_m)$ with a model that treats the bed as a porous piston with permeability k. We consider two parts of the free-flight portion during each shaking cycle (vertical lines in Fig. 4): In part I, gas flows down into the gap opened up at the cell bottom and produces a drag that adds to the gravitational acceleration g. In part II, the gap closes, so that the gas pushed upward through the bed creates a drag force opposing the inertial force.

We approximate both the packing fraction ϕ of bed particles and the pressure gradient to be constant throughout. A more detailed discussion will be presented elsewhere [18]. By Darcy's law, incompressible gas of viscosity μ and velocity u flowing through the bed produces a pressure gradient $\partial P/\partial z = \mu u/k$. This leads to a drag force $(\mu u/k)V$ on a bed volume V. At the same time, an intruder of volume V_i experiences a force $F_d = \oint_i P(z)dS = (\partial P/\partial z)V_i = (\mu u/k)V_i$ that can be a significant fraction of its weight. Using appropriate values for μ and k [18], we find $0.3 < F_d/(mg) < 40$ depending on

intruder density. Consider the free-flight motion of an intruder of mass $m_i = \rho V_i$ relative to a neighboring, identical volume V_i composed only of bed material. Depending on whether the sign of the mass difference $\Delta m = (\rho - \phi\rho_m)V_i$ between the two volumes is positive (negative), the intruder during part I will push against the material above (below) it. We calculate the net force on the compound object consisting of the intruder and the vertical column (diameter D) of bed material either above or below it. We find that, during part I, intruders with $\rho/\rho_m < \phi$ will sink, while those with $\rho/\rho_m > \phi$ will rise relative to the neighboring bed.

During part II of the free flight the situation changes. Now the heavy (light) intruder accelerates together with the column of material below (above) it. Because inertial and drag forces oppose each other, light intruders experience smaller acceleration magnitudes and fall more slowly than the surrounding bed. In particular, near the top surface light intruders can reach their terminal velocity before the bed collides with the base. We see evidence of this in the inset of Fig. 4(a) as the parabolic trajectory changes to a linear, constant velocity segment in the lab frame. Finally, we assume that any gap around the intruder is immediately filled by bed particles so that its displacement over one shaking cycle is the sum of the displacements from parts I and II.

From these considerations several predictions emerge. First, at $\rho^*/\rho_m = \phi$ the intruder experiences no motion relative to the bed. This is what is seen in Fig. 1(c) and in the smooth cell leads to a divergence in T_{rise}. In the presence of convection, this divergence should be cut off by the convective rise time. Second, the peak in T_{rise} should occur at a packing fraction corresponding to a loosely packed "in-flight" bed configuration. This explains similar values $\rho^*/\rho_m \sim 0.5$ even if bed particle sizes and shaking parameters differ [8–10]. Third, for light intruders the amount of sinking during part I and rising during part II should depend on their vertical position in the bed. Thus, for $\rho/\rho_m < \phi$ there should be a critical initial height, h_c, separating rising and sinking behaviors. Because convection will produce a bias towards rising, it will reduce h_c in the rough cell. Qualitatively, this explains the key features of the phase diagrams in Fig. 3. Finally, the model implies that the sinking found by us and others [6,7] depends on a pressure gradient and should vanish in vacuum, where only the convection-driven, density-independent rising effect survives [5]. This is confirmed by the data in Fig. 2.

While the above model provides a mechanism for the demise of the density dependence with decreasing pressure it neglects a number of aspects that might be important: variation in $\partial P/\partial z$, compressibility of the bed and associated variations of ϕ with position, and pressure dependence of convection. Thus, the model cannot predict the detailed shape of the phase diagram (Fig. 3) nor the inset of Fig. 2(a). From earlier results [19] by the Duke group, we would have expected a significant pressure dependence only once P approached values close to 2 kPa. However, our results clearly demonstrate changes in the behavior at much larger P.

Our phase diagram shows that previous perplexing results obtained by different groups [5–10] belong to different regimes of the same phenomenon. Using MRI and high-speed video, we found the underlying mechanisms of the density-dependent behavior of intruders. Moreover, a simple model can give a qualitative description of the key experimental results.

We thank N. Mueggenburg and E. Corwin for fruitful discussions, J. Rivers for MRI support, and Peter Eshuis for help with the experiment. This work was supported by the NSF under CTS-0090490, and MRSEC, DMR-0213745, and by DOE under W-7405-ENG-82. M. E. M. acknowledges support from the Burroughs-Wellcome Foundation.

[1] A. Kudrolli, Rep. Prog. Phys. **67**, 209 (2004).
[2] H. M. Jaeger, S. R. Nagel, and R. P. Behringer, Rev. Mod. Phys. **68**, 1259 (1996).
[3] A. Rosato, K. J. Strandburg, F. Prinz, and R. H. Swendsen, Phys. Rev. Lett. **58**, 1038 (1987).
[4] J. Duran, J. Rajchenbach, and E. Clement, Phys. Rev. Lett. **70**, 2431 (1993).
[5] J. B. Knight, H. M. Jaeger, and S. R. Nagel, Phys. Rev. Lett. **70**, 3728 (1993).
[6] T. Shinbrot and F. J. Muzzio, Phys. Rev. Lett. **81**, 4365 (1998).
[7] X. Yan *et al.*, Phys. Rev. Lett. **91**, 014302 (2003).
[8] M. Möbius, B. E. Lauderdale, S. R. Nagel, and H. M. Jaeger, Nature (London) **414**, 270 (2001).
[9] M. Rhodes, S. Takeuchi, K. Liffman, and K. Muniandy, Granular Matter **5**, 107 (2003).
[10] D. A. Huerta and J. C. Ruiz-Suárez, Phys. Rev. Lett. **92**, 114301 (2004); **93**, 069901(E) (2004).
[11] D. C. Hong, P. V. Quinn, and S. Luding, Phys. Rev. Lett. **86**, 3423 (2001).
[12] A. P. J. Breu, H.-M. Ensner, C. A. Kruelle, and I. Rehberg, Phys. Rev. Lett. **90**, 014302 (2003).
[13] N. Burtally, P. J. King, and M. R. Swift, Science **295**, 1877 (2002).
[14] K. Liffman *et al.*, Granular Matter **3**, 205 (2001).
[15] M. A. Naylor, M. R. Swift, and P. J. King, Phys. Rev. E **68**, 012301 (2003).
[16] L. Trujillo and H. J. Herrmann, Physica (Amsterdam) **330A**, 519 (2003).
[17] B. Thomas and A. M. Squires, Phys. Rev. Lett. **81**, 574 (1998); Powder Technol. **100**, 200 (1998).
[18] M. Möbius *et al.* (to be published).
[19] H. K. Pak, E. Van Doorn, and R. P. Behringer, Phys. Rev. Lett. **74**, 4643 (1995).